Forum geografic. Studii și cercetări de geografie și protecția mediului
Volume **XXV**, Issue **1** (**June 2026**), pp. **43-57;** DOI: **10.5775/fg.2026.1.3768**

Geomorphological mapping of steep new vineyard terraces: DJI Mavic 3M vs. Matrice T4 RTK performance with and without GCPs

Jesús GONZÁLEZ-VIVAR[1], Laura CAMBRONERO-RUÍZ[1,2], Maria Teresa GONZÁLEZ-MORENO[1,2], Jesús RODRIGO-COMINO[1,2,*]

[1] Departamento de Análisis Geográfico Regional y Geografía Física, Facultad de Filosofía y Letras, Campus Universitario de Cartuja, University of Granada, 18071 Granada, Spain
[2] Andalusian Research Institute in Data Science and Computational Intelligence, University of Granada, 18016 Granada, Spain
* *Corresponding author*: jesusrc@ugr.es

Received on 06-06-2026, reviewed on 26-06-2026, accepted on 30-06-2026

Abstract

Soil erosion in steep vineyard terraces presents critical environmental challenges that require high-resolution, real-time geomorphological monitoring. Unmanned Aerial Vehicle (UAV) photogrammetry has revolutionized this field; however, an experimental gap persists regarding the operational need for Ground Control Points (GCPs) when utilizing high-precision Real-Time Kinematic (RTK) systems in extreme geometries. This study provides a rigorous comparative analysis between the DJI Mavic 3M and the DJI Matrice T4 (Thermal) platforms under two georeferencing configurations (RTK-only direct georeferencing vs. RTK+GCP workflows). Both drones were operated under identical parameters: flown on the same day at solar noon, with an 80% longitudinal and lateral image overlap, and at a flight altitude of 40 m above ground level. Four key topographic and soil erosion derivatives were extracted in ArcGIS Pro and statistically compared cell-by-cell using raster calculator algebra: Slope Gradient, Topographic Wetness Index (TWI), Convergence Index (CI), and the RUSLE LS-factor. The residual analysis revealed an outstanding structural alignment between workflows, with absolute median discrepancies restricted to 0.7° for slope, 0.4 for TWI, and 0.0 for CI. Absolute coordinate tracking across 10 independent checkpoints unveiled that the non-GCP workflow behaves as a perfectly rigid photogrammetric block, introducing an identical systematic translation vector (Delta X= 0.2 m, Delta Y= 5.4 m, Delta Z= -2.8 m) with near-zero standard deviations (approx. 0.1 m) for both platforms. Because neighborhood-cell algorithms remain unaffected by this rigid displacement, the derivative geomorphological maps are morphologically identical. These findings demonstrate that for high-resolution pedogeomorphological monitoring on steep slopes, the internal positioning stability of the DJI D-RTK 3 system successfully eliminates the operational dependency on physical ground control networks. This methodological shift significantly optimizes fieldwork efficiency, safety, and operational costs without compromising scientific rigor.
Keywords: *UAV photogrammetry, RTK direct georeferencing, terraced vineyards, geomorphological mapping, soil erosion modeling*

Introduction

Soil erosion in vineyards represents one of the most critical environmental challenges in Mediterranean and steep-slope agricultural landscapes (Prosdocimi et al., 2016; Rodrigo-Comino, 2018). The intensive management of these areas to obtain the highest high quality production, combined with continuous tillage with bare soil maintenance, severely accelerates soil erosion and alters hydrological responses (Andrenelli et al., 2025; Gholamahmadi et al., 2025). This acceleration triggers immediate surface runoff, which drives severe associated processes such as the depletion of vital soil nutrients, the mitigation and release of organic carbon into the atmosphere, and a systemic reduction in soil organic matter (Bogunovic et al., 2020; Novara et al., 2011). There is an urgent need to identify, monitor, and implement sustainable management practices capable of mitigating erosion rates, preserving soil structural integrity, and enhancing ecosystem resilience against climate-induced degradation (Caffaro et al., 2024; Gall et al., 2025).

In recent decades, significant advancements in geomorphology, soil geography, and pedogeomorphology have transformed how hillside stability and degradation dynamics are evaluated, primarily driven by developments in remote sensing (Pawlik, 2025; Trevisani & Guth, 2025). Among these technologies, Unmanned Aerial Vehicles (UAVs) have emerged as a revolutionary tool, enabling real-time, ultra-high-resolution monitoring and quantification of active geomorphological processes (Alexiou et al., 2023; Eltner et al., 2013). The integration of modern Real-Time Kinematic (RTK) positioning systems within UAVs, coupled with ground truth validation using Global Positioning Systems (GPS), has exponentially increased the spatial accuracy of digital elevation models (Bertin et al., 2022; Tan et al., 2024). Nevertheless, an experimental gap persists in international literature: it remains unclear which specific drone platforms and under what precise operational conditions can deliver the most accurate geomorphological maps, especially when balancing technological configurations (Rodrigo-Comino et al., 2026).

In the specific context of viticulture, the construction of terraced systems has historically allowed the cultivation of steep slopes that would otherwise be topographically impracticable (Blavet et al., 2009; Ramos & Porta, 1997). However, numerous authors have demonstrated that these human-modified landforms frequently reach the highest rates of soil erosion (Chen et al., 2017). In the Iberian Peninsula, seminal works by Romero-Díaz et al. (2017a) in the Murcia region, Martínez-Casasnovas et al. (2016) in the Penedès region, and Rodrigo-Comino et al. (2019) in the Málaga province have highlighted how terrace abandonment, structural failure, and lack of vegetative cover trigger catastrophic soil loss. Furthermore, on an international scale, researchers in Italy have successfully started UAV photogrammetry in Italian terraced vine-yards to detect and track the development of severe gully erosion and bank failures, confirming the vulnerability of these agricultural systems (Pijl et al., 2019).

Despite the extensive literature on vineyard erosion, a critical methodological question remains unanswered: What is the optimal workflow to produce highly accurate geomorphological maps in steeply terraced vineyards? Specifically, does the combination of RTK positioning with Ground Control Points (GCPs) significantly outperform a pure RTK direct georeferencing approach without GCPs, or can the latter achieve sufficient accuracy for geomorphological map-ping? Moreover, how does platform choice influence this accuracy? To address this gap, this study provides a rigorous comparative analysis between two distinct UAV platforms supported by a RTK positioning system: the lightweight DJI Mavic 3M and the DJI Matrice T4. Both systems were tested with and without GCPs under strictly controlled experimental conditions: flown on the same day, at identical times to minimize shading varia-tions, using an 80% forward and side overlap, and at a constant flight altitude of 40 meters above ground level.

Materials and methods

Study area

The study area (Fig. 1) is located in a recently established vineyard in the municipality of Los Guájares, in the province of Granada (Andalusia, southern Spain). The vineyard belongs to Bodegas Calvente and is located at UTM coordinates ETRS89 Zone 30N (X: 445371; Y: 4075046). The experimental plot ranges in elevation from 1020 m to 1073 m a.s.l., corresponding to the highest terrace.

The study plot covers an area of 2.59 ha and corresponds to a newly planted vineyard established in May 2026 on a recently created agricultural terrace system. These cultivation structures are adapted to an environment of high topographical complexity, characteristic of the mountainous areas in the southern province of Granada, where the transformation of the relief through terraces allows the implementation of woody crops in areas with steep slopes (Durán-Zuazo & Rodriguez, 2008). The terraced configuration of the terrain creates a scenario of interest for the application of remote sensing techniques due to the potential existence of spatial variations associated with factors such as solar exposure, edaphic characteristics, water availability, and microclimatic conditions (Preti & Romano, 2014).

From a physiographic point of view, the study area is located within the setting of the Penibaetic System (Cordillera Penibética), inside a mountainous agricultural landscape characterized by irregular relief and high spatial heterogeneity (García-Ruiz, 1988). The terraced hillslope shows a homogeneous northwestern orientation. While the inner cultivated benches maintain an approximate average slope of 5% to optimize water management, the structural terrace risers and global hillslope topography present steep gradients that aver-age 22°–23° and reach sub-vertical inclinations. These topographical features condition the distribution of incident radiation and the processes related to the sur-face energy balance, factors that can influence the spec-tral and thermal response of the vegetation obtained via remote sensors (Jenerowicz et al., 2023; Farella et al., 2022).

Despite being located at a high altitude, the plot is relatively close to the Mediterranean coast, being approximately 8 km in a straight line from the nearest beach, located in the coastal area of Salobreña (Granada). This geographical position creates a transition between environmental conditions typical of mountainous areas and the maritime influence of the Granadan Costa Tropical. This combination of factors favors conditions characterized by high solar radiation availability, daily thermal amplitude, and a marked Mediterranean character, which are relevant aspects in the development and physiological behavior of the vineyard crop (Costa et al., 2023; Barbera & Cullotta, 2016).

The vineyard is composed of four grapevine varieties, corresponding to three white (Chardonnay, Vigiriego, and Riesling) and one red (Petit Verdot). Due to its recent establishment, the plot is in an initial stage of vegetative development.

At the time of the study, the crop did not have an installed irrigation system, although its incorporation is planned for later stages of the plantation's development, estimated for the coming month. The planting pattern presents a layout of 1.1 m vine spacing and 2.30 m inter-row spacing. At the time of the study, the plot showed a total absence of vegetative cover, characterized by completely bare soil due to the recent land preparation for planting.

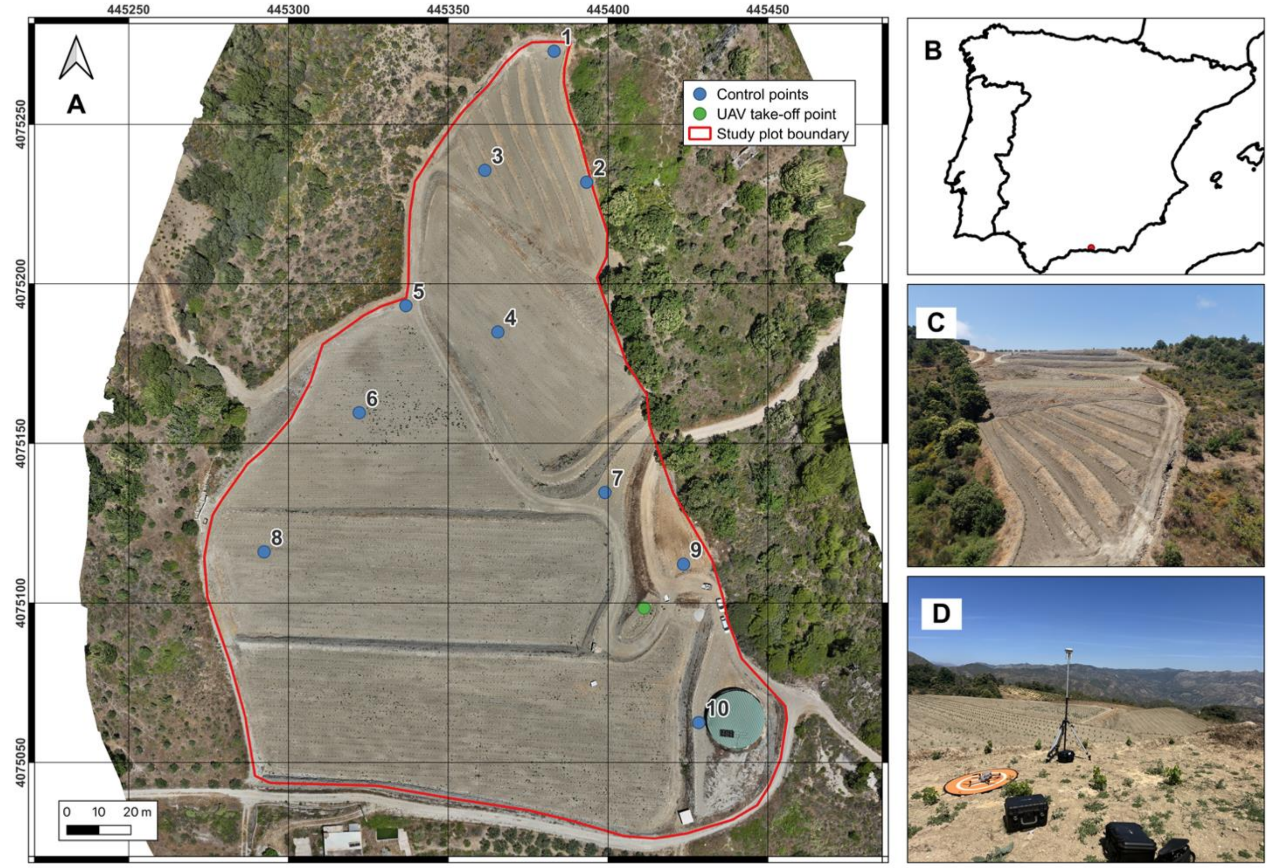

Figure 1. Localization of the study area: (a) high-resolution orthophoto, including the Ground Control Points (GCPs); (b) location of the study plot in southern Spain; (c) panoramic view of the study plot (DJI MiniPro 5); (d) UAV take-off point, situated at the highest elevation of the study plot and RTK positioning system (1,073 m a.s.l.)

Flight campaigns and photogrammetric parameters

To ensure strict experimental consistency and minimize environmental variables, both Unmanned Aerial Vehicle (UAV) flight campaigns were carried out on the same day under identical atmospheric conditions. The missions were synchronized at 12:00 PM (local solar noon) to maximize the solar elevation angle, thereby minimizing shadows cast by the steep terrace risers and ensuring optimal, uniform illumination across the complex topography. Both platforms were operated using automated flight planning software to execute a grid pattern with an 80% frontal (longitudinal) and 80% lateral (transverse) image overlap (DJI Pilot 2). The flight altitude was rigidly maintained at 40 meters above ground level (AGL) relative to the take-off point, balancing high spatial resolution with operational safety in the steep terrain.

Two distinct multi-rotor UAV platforms representing different weight classes and payload configurations were evaluated (Fig. 2):

• DJI Mavic 3 Multispectral (Mavic 3M): A lightweight, compact enterprise drone (take-off weight of 951 g) equipped with an integrated RTK module. For this study, the primary RGB sensor was utilized, featuring a 4/3-inch CMOS sensor with 20 megapixels (MP) and a mechanical shutter to prevent motion blur during high-speed flight.

• DJI Matrice T4 (Thermal): A high-stability industrial enterprise platform equipped with native RTK positioning. For the photogrammetric and geomorphological reconstruction, the primary high-resolution RGB optical sensor integrated into the thermal payload camera system was utilized, operating under identical overlap and altitude constraints.

Figure 2. UAV platforms used in the study

Georeferencing, Base Stations, and Ground Control

To evaluate the absolute and relative spatial accuracy of the geomorphological products under different constraints, a dual-scenario framework (with and without Ground Control Points) was implemented using high-precision Global Navigation Satellite Systems (GNSS).

Real-time kinematic corrections during the flights were provided by a DJI D-RTK 3 High-Precision GNSS Mobile Station, which simultaneously tracks multiple satellite constellations (including GPS, GLONASS, Galileo, and BeiDou). The station was set up over a known local control point to broadcast differential corrections directly to both the Mavic 3M and Matrice T4 via data links, guaranteeing centimeter-level real-time positioning accuracy.

For ground truth validation and the implementation of the GCP-backed scenarios, a network of ten artificial targets was distributed across the new steep terraced vineyard. The precise three-dimensional coordinates (X,Y,Z) were measured using an Emlid Reach RS3 multi-band GNSS receiver equipped with an Inertial Measurement Unit (IMU) for tilt compensation. The receiver tracked GPS/QZSS, GLONASS, BeiDou, and Galileo signals to achieve maximum accuracy. The raw geodetic data collected by the receiver was managed, verified, and post-processed using the Emlid Flow software ecosystem to guarantee maximum coordinate reliability. These points were systematically split into Ground Control Points (GCPs) for block adjustment optimization.

Data processing and photogrammetric pipeline

The raw digital imagery and embedded EXIF/XMP metadata (including the high-precision RTK geotags) from both drone flights were imported into Esri ArcGIS Drone2Map (Colorado, USA) software for photogrammetric reconstruction. The processing workflow followed a standardized structure divided into two primary georeferencing configurations:

- RTK-Only Scenario: The structural block adjustment was computed relying exclusively on the camera positions georeferenced by the DJI D-RTK 3 station, treating the field-measured targets strictly as independent checkpoints to validate the vertical and horizontal errors.
- RTK + Ten GCP Scenario: The block adjustment was optimized by manually identifying and binding the Emlid-surveyed GCPs within the image matching pipeline, refining the camera calibration parameters and interior orientation.

For both scenarios, the initial tie-point generation, bundle block adjustment, and dense point cloud densification were executed at full resolution. The final outputs generated for geomorphological interpretation and comparative analysis included ultra-high-resolution Digital Surface Models (DSMs), and orthomosaics.

Geomorphometric maps and geostatistical comparison

To evaluate how platform choice and georeferencing configurations impact the geomorphological characterization of new steep vineyard terraces, a comprehensive geomorphometric and geostatistical pipeline was implemented in Esri ArcGIS Pro following previous works (Cambronero et al., 2025; González-Moreno & Rodrigo-Comino, 2025). Four distinct digital elevation scenarios were analyzed: (1) Mavic 3M RTK-only, (2) Mavic 3M RTK+GCP, (3) Matrice T4 RTK-only, and (4) Matrice T4 RTK+GCP. The raw filtered photogrammetric Digital Surface Models (DSMs) were standardized to a common spatial resolution to ensure spatial compatibility (GSD: 1 cm). Four critical terrain attributes for soil erosion and hydrological modeling were computed using the Spatial Analyst toolbox in ArcGIS Pro:

- Slope Gradient (Degrees): Calculated using the Surface Parameters tool. The algorithm computes the maximum rate of change in elevation from each cell to its neighbors using a bivariate quadratic local surface fitting. This method provides smoother, more realistic derivatives on highly complex, steeply terraced slopes compared to traditional neighborhood methods.
- Topographic Wetness Index (TWI; (Kopecký et al., 2021): It quantifies topographic control on hydrological processes and potential runoff accumulation areas. It was computed via the Raster Calculator using the standard formula:

$$TWI = \ln\left(\frac{\alpha}{\tan(\beta)}\right)$$

where α is is the specific catchment area (local contributing area per unit contour length) derived from a D8 flow accumulation routing algorithm after hydrologically conditioning the DTM (filling sinks), and β is the slope gradient in radians.

- Convergence Index (CI): The CI was generated to identify flow convergence (valleys/gullies) and divergence (ridges/terrace risers) structures (Arabameri et al., 2018). The index evaluates the average aspect difference between a central cell and its eight surrounding neighbors. Negative values indicate convergent terrain configurations prone to concentrated runoff, while positive values represent divergent structures.
- LS Factor (RUSLE):The combined slope length (*L*) and slope steepness (*S*) factor from the Revised Universal Soil Loss Equation (RUSLE) was calculated to model topographic susceptibility to soil erosion. The extraction followed an algorithm (Desmet & Govers, 1996), which accounts for complex 3D surfaces and flow convergence:

- $LS = L_{i,j} \cdot S_{i,j}$

where the *L* factor computes the upstream contributing area for each specific pixel (i,j) adjusting for slope changes, and the *S* factor addresses the non-linear acceleration of velocity on steep slopes.

To quantitatively assess the internal consistency and absolute structural deviations between the photogrammetric configurations, a dual-layer statistical comparison was performed. The Raster Calculator tool was utilized to generate cell-by-cell Difference of Elevation maps with 10 known points registering X, Y and Z coordinates. This allowed for the spatial identification of where the largest geometric mismatches occurred (e.g., whether errors clustered on vertical terrace walls, inner channels, or flat vine rows). Spatial structural continuity and spatial dependence of the errors and geomorphometric indices were examined using experimental variograms, transformed into boxplots to graphically observe the differences.

Comparing the variogram parameters (datasets and tables) between the RTK-only and RTK+GCP configurations for both the Mavic 3M and Matrice T4 allowed to identify whether omitting Ground Control Points introduces systemic spatial distortions (tilt or warping) or increases random high-frequency noise across the terraced landscape.

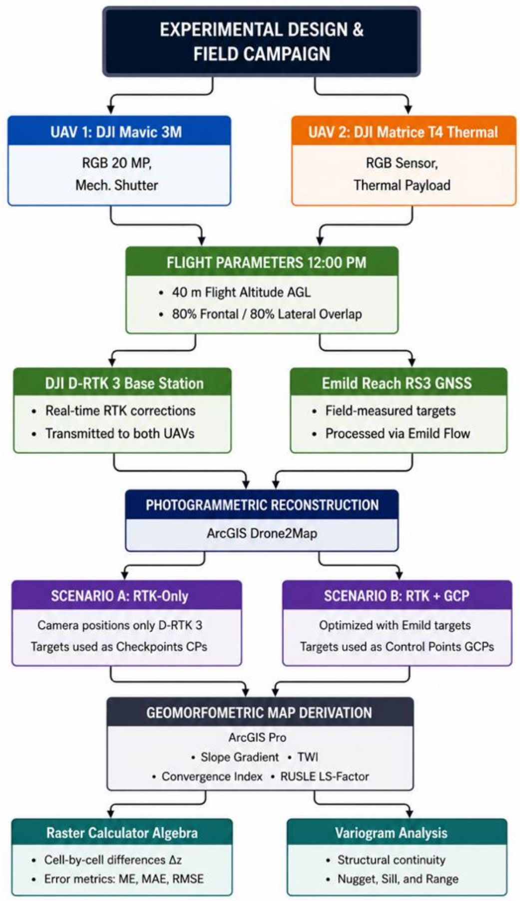

Figure 3. Methodological workflow

Results

Photogrammetric processing performance

Before evaluating the geomorphological products derived from the digital surface models, the quality of the four photogrammetric reconstructions was assessed to ensure that the resulting datasets were generated under comparable processing conditions (Table 1).

The comparison included the main quality indicators provided by Drone2Map, encompassing project characteristics, image calibration statistics, bundle adjustment performance, camera optimization and image position corrections. These parameters provide an overview of the geometric quality of each photogrammetric block and allow the influence of Ground Control Points (GCPs) on the image adjustment to be evaluated prior to the terrain analysis.

Table 1 summarizes the main processing statistics obtained for the four photogrammetric projects. Complete image calibration was achieved in every case, with all acquired photographs successfully oriented during the bundle adjustment (679 images for the DJI Mavic 3 Multispectral and 2,209 images for the DJI Matrice T4). Likewise, mission size, covered area and mean Ground Sampling Distance (GSD) remained identical between the processing performed with and without GCPs for each UAV platform, confirming that both processing strategies were directly comparable.

The internal quality indicators of the bundle adjustment showed only minor differences between processing strategies. The DJI Mavic 3 Multispectral maintained a Tie Point Mean Reprojection Error (RMSE) of 0.20 pixels irrespective of GCP incorporation, whereas the DJI Matrice T4 exhibited a slight reduction from 0.27 pixels to 0.24 pixels after the inclusion of the ten ground control points.

Similarly, the mean number of tie points per solution point varied only marginally, increasing from 6.56 to 6.63 in the Mavic 3M dataset and from 8.92 to 8.93 in the Matrice T4 dataset. Camera self-calibration remained highly stable for both sensors, with focal length optimization values below 1% in all cases.

The incorporation of GCPs enabled the estimation of absolute positioning residuals during the adjustment. The DJI Mavic 3 Multispectral achieved RMSE values of 0.025 m, 0.022 m and 0.012 m for the X, Y and Z coordinates, respectively, whereas the DJI Matrice T4 recorded corresponding values of 0.045 m, 0.039 m and 0.029 m.

The maximum orientation uncertainties remained below 0.014 m for positional parameters and below 0.006° for angular parameters across all four projects, indicating stable bundle adjustment solutions.

In the RTK-only processing, the differences between the initial and adjusted camera positions were negligible. Conversely, for the projects processed with GCPs, the bundle adjustment resulted in systematic differences between the initial RTK camera positions and the final adjusted positions, with average values of approximately −0.17 m, −5.3 m and +2.8 m along the X, Y and Z components, respectively, for both UAV platforms.

Table 1. Statistical datasets obtained from each flight and images processing using Drone2map-exported reports

Category	Parameter	M3 RTK	M3 RTK + GCPs	MT4 RTK	MT4 RTK + GCPs
Project characteristics	Images calibrated	679/679	679/679	2209/2209	2209/2209
	Mission size (GPx)	14.0	14.0	26.0	26.0
	Coverage area (ha)	9.1	9.1	8.2	8.2
	Mean GSD (m)	0.013	0.013	0.017	0.017
	Processing time	2h30m	1h44m	2h38m	4h21m
Bundle adjustment	Tie Point RMSE (px)	0.20	0.20	0.27	0.24
	Mean tie points / solution point	6.56	6.63	8.92	8.93
	Focal length optimization (%)	0.10	0.10	0.71	0.71
	Maximum orientation uncertainty X (m)	0.002	0.005	0.001	0.006
	Maximum orientation uncertainty Y (m)	0.002	0.005	0.001	0.006
	Maximum orientation uncertainty Z (m)	0.001	0.008	0.000	0.014
	Maximum Ω uncertainty (°)	0.004	0.006	0.001	0.005
	Maximum Φ uncertainty (°)	0.003	0.006	0.001	0.005
	Maximum K uncertainty (°)	0.002	0.002	0.001	0.003
Image position correction	Mean ΔX (m)	0.000	−0.172	0.000	−0.128
	Mean ΔY (m)	0.000	−5.310	0.000	−5.368
	Mean ΔZ (m)	0.000	+2.787	0.000	+2.817
Ground control	Number of GCPs	0	10	0	10
	RMSE X (m)	—	0.025	—	0.045
	RMSE Y (m)	—	0.022	—	0.039
	RMSE Z (m)	—	0.012	—	0.029

Geomorphometric products and statistical comparison of the DSMs

Table 2. Descriptive statistics of cell-by-cell slope dis-crepancies (in degrees) between DJI Mavic 3M and DJI Matrice T4 photogrammetric derivatives under different georeferencing configurations (With GCPs vs. Without GCPs), including abso-lute differences and relative variance changes (%)

Parameter	With GCPs	Without GCPs	Difference	Relative change (%)
Mean	1.3	1.3	0.6	2.0
Median	0.5	2.3	0.7	3.0
Minimum	0.0	0.0	0.0	—
Maximum	89.8	89.8	0.0	0.0
Standard deviation	21.9	22.0	0.1	0.6
Coefficient of variation (%)	78.6	77.5	−1.1	−1.4
Percentile 5 (P5)	2.9	3.0	0.1	5.1
Percentile 25 (P25)	8.6	9.1	0.5	5.3
Percentile 75 (P75)	43.0	43.6	0.6	1.5
Percentile 95 (P95)	70.6	71.5	0.9	1.3

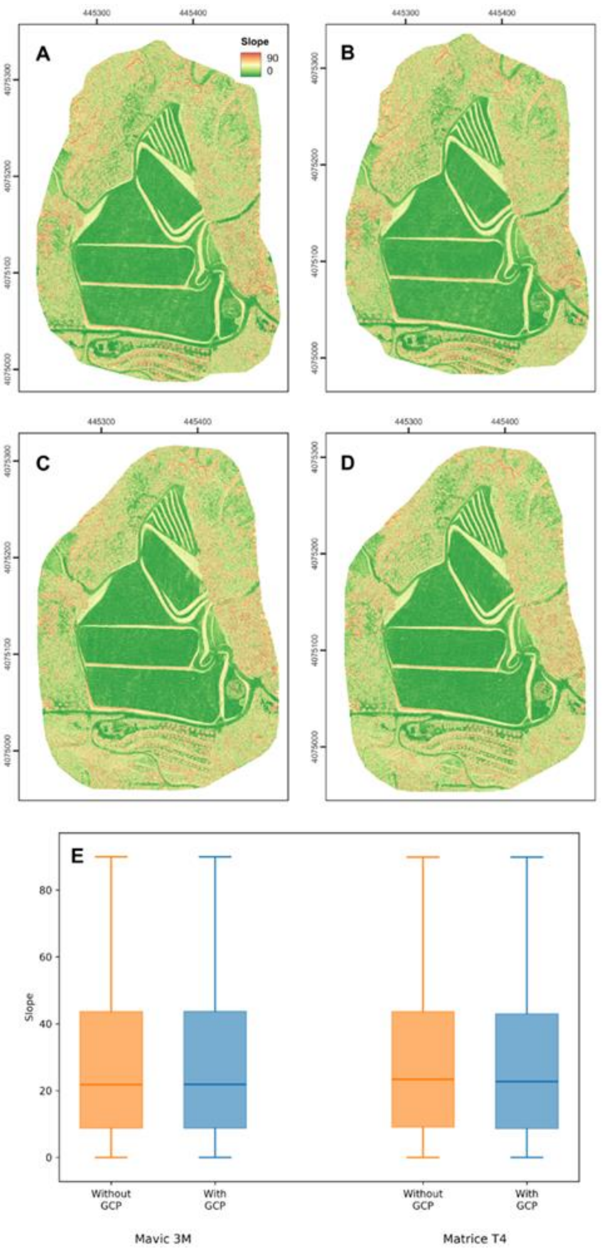

Figure 4. Comparison of slope maps (degrees) and statistical distributions obtained from the four UAV photogrammetric workflows using RTK direct georeferencing and RTK combined with Ground Control Points (GCPs). (A) DJI Mavic 3 Multispectral (RTK only); (B) DJI Mavic 3 Multispectral (RTK + GCPs); (C) DJI Matrice T4 (RTK only); (D) DJI Matrice T4 (RTK + GCPs); (E) Boxplot comparison of slope distributions

The spatial and statistical consistency between the geomorphometric layers was evaluated through a cell-by-cell raster subtraction of the slope gradients derived from the DJI Mavic 3M and DJI Matrice T4 platforms. As synthesized in Figure 4 and Table 2, the residual analysis demonstrates an exceptionally high geometric alignment between both UAV systems, confirming that next-generation RTK positioning minimizes structural warping in steep terraced environments. When both platforms were optimized using the Ground Control Point network ("With GCPs"), he mean slope discrepancy was 1.3°, with an absolute difference between configurations of just 0.6° (Table 2).

In the direct georeferencing scenario where ground control targets were omitted ("Without GCPs"), the mean discrepancy remained perfectly stable at 1.3°, while the median variation experienced a subtle increase to 2.3°. This operational shift results in an absolute median difference of 0.7°, which corresponds to a minor relative change of only 3.0% in the internal topographic variance between the two flights. The distribution of the elevation derivatives across the different topographic percentiles further supports the reliability of the non-GCP workflow. In the lower and intermediate slope intervals (P5 to P25), the absolute differences between the workflows do not exceed 0.5°.

Even when evaluating the most complex features of the landscape—such as the sub-vertical terrace risers represented by the upper percentiles—the deviations remain negligible; the 75th percentile (P75) shifts by only 0.6° (from 43.0° to 43.6°) and the 95th percentile (P95) shows a variation of 0.9° (moving from 70.6° to 71.5°). The maximum recorded slope gradient (89.8°) and the overall standard deviation (~22.0°) remained virtually identical across all configurations, displaying a minimal relative change of 0.6%.

Table 3. Descriptive statistics of cell-by-cell RUSLE LS-factor discrepancies between DJI Mavic 3M and DJI Matrice T4 photogrammetric models under different georeferencing configurations (With GCPs vs. Without GCPs), including absolute differences and relative changes (%)

Parameter	With GCPs	Without GCPs	Difference	Relative change (%)
Mean	1.3	1.3	0.0	0.8
Median	0.5	0.5	0.0	−0.3
Minimum	0.0	0.0	0.0	—
Maximum	1636.5	1548.0	−88.5	−5.4
Standard deviation	7.1	6.9	−0.1	−1.9
Coefficient of variation (%)	553.0	538.3	−14.7	−2.7
Percentile 5 (P5)	0.0	0.0	0.0	—
Percentile 25 (P25)	0.1	0.1	0.0	−3.5
Percentile 75 (P75)	1.4	1.4	0.0	−0.5
Percentile 95 (P95)	4.0	4.0	0.0	0.9

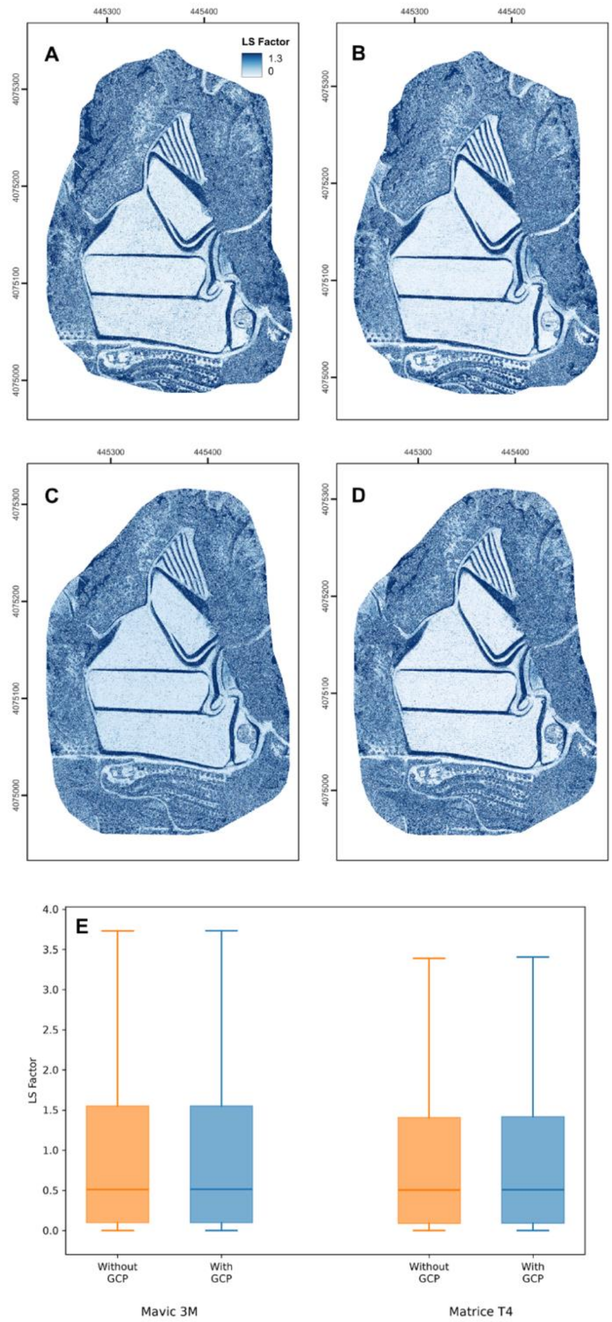

Figure 5. Comparison of LS factor maps and statistical distributions obtained from the four UAV photogrammetric workflows using RTK direct georeferencing and RTK combined with Ground Control Points (GCPs). (A) DJI Mavic 3 Multispectral (RTK only); (B) DJI Mavic 3 Multispectral (RTK + GCPs); (C) DJI Matrice T4 (RTK only); (D) DJI Matrice T4 (RTK + GCPs); (E) Boxplot comparison of LS factor distributions

The spatial compliance of the soil erosion modeling parameters was evaluated through a cell-by-cell raster subtraction of the slope length and steepness (*LS*) factor maps generated by the DJI Mavic 3M and DJI Matrice T4 platforms (Fig. 5 and Table 3). Visually, the spatial distribution of the *LS* factor remains completely homogeneous across all four configurations, consistently mapping minimal values on the flat terrace benches and identifying increased erosion susceptibility along the steep terrace risers.

The geostatistical comparison of the residuals demonstrates that the choice of UAV platform and the omission of physical ground control targets introduce negligible variation in the structural core of the erosion models.

When analyzing the absolute differences under both configurations ("With GCPs" and "Without GCPs"), the mean discrepancy between the two drone systems was confined to 1.3, with a median variation of just 0.5 in both workflows. The absolute difference between the two operational scenarios for both the mean and median was mathematically zero, displaying a minimal relative change of –0.3% in the median structural alignment.

This exceptionally high geometric synchronization between the Mavic 3M and Matrice T4 is further confirmed across the lower and intermediate topographic percentiles (P5, P25, and P75), where the absolute difference between having or not having a GCP network remains fixed at 0.0. Even at the extreme upper boundaries of the landscape dynamics—represented by the 95th percentile (P95)—the spatial discrepancy between platforms shifts by a negligible in absolute terms, translating to a minor relative change of only 0.9% shifts by a negligible 0.0 in absolute terms.

Conversely, localized maximum discrepancies reached outlier peaks of 1636.5 (With GCPs) and 1548.0 (Without GCPs), yielding an absolute maximum difference of –88.5. These localized errors, which account for the exceptionally high coefficients of variation (553%), represent mathematical artifacts induced by the D8 flow accumulation routing algorithm on the extreme edges of the photogrammetric blocks. Because these edge effects are completely unrelated to actual slope morphology or landform features, they were filtered out of the cartographic legends (Fig. 5A–D) as commanded to preserve map legibility. The exploratory boxplot distribution (Fig. 5E) visually records these findings: the interquartile ranges (IQR) and median lines are identically positioned across all four scenarios.

The spatial distribution of the Topographic Wetness Index (TWI) was mapped to assess how platform constraints and ground control configurations impact the delineation of potential runoff accumulation zones (Fig. 6 and Table 4).

The spatial patterns of hydrological convergence and divergence remain highly uniform across all four generated models, clearly distinguishing the drier, well-drained conditions of the sub-vertical terrace risers from the localized accumulation pathways situated along the inner terrace benches.

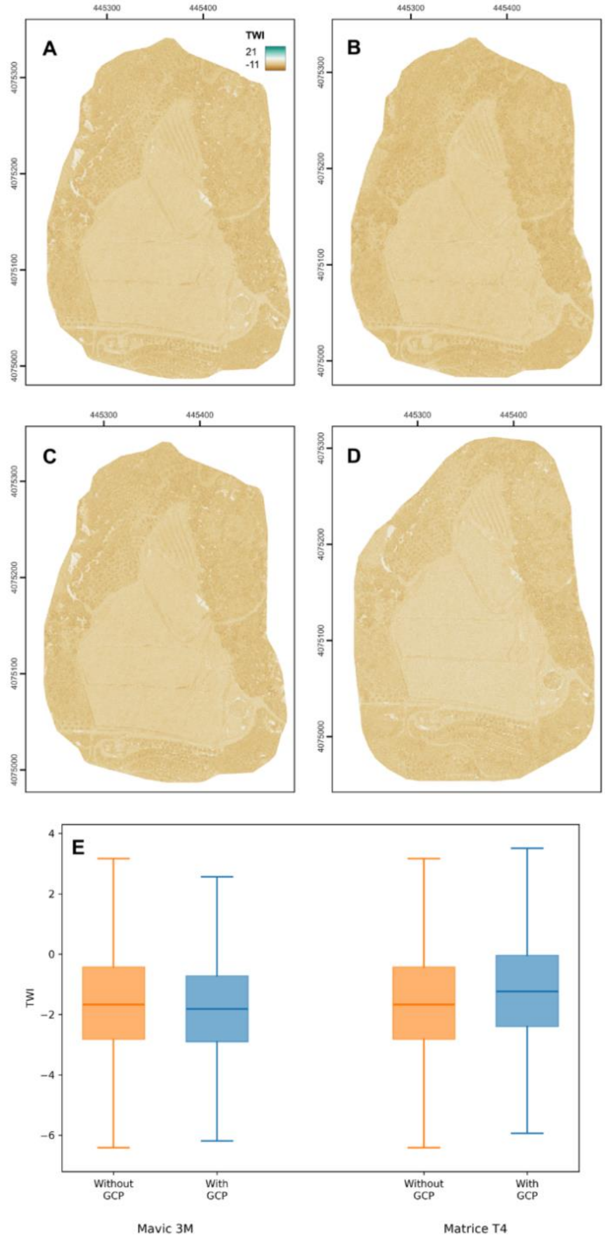

Figure 6. Comparison of Topographic Wetness Index (TWI) maps and statistical distributions obtained from the four UAV photogrammetric workflows using RTK direct georeferencing and RTK combined with Ground Control Points (GCPs). (A) DJI Mavic 3 Multispectral (RTK only); (B) DJI Mavic 3 Multispectral (RTK + GCPs); (C) DJI Matrice T4 (RTK only); (D) DJI Matrice T4 (RTK + GCPs); (E) Boxplot comparison of Topographic Wetness Index (TWI) distributions

The geostatistical comparison of the TWI residuals establishes that bypassing the ground control network yields minimal absolute structural variation. Under a fully controlled workflow ("With GCPs"), the mean cell-by-cell TWI discrepancy between the DJI Mavic 3M and DJI Matrice T4 was restricted to –1.1, while shifting slightly to –1.5 in the direct direct-georeferencing approach ("Without GCPs"). This variance yields a minor absolute difference of just –0.4. While the relative change metrics register high percentages in certain sectors—such as the 37.8% in the mean or the anomalous 1032.1% in the 75th percentile (P75)—these values represent statistical amplification artifacts induced by dividing minor absolute variances by baselines near or at the zero threshold.

The exploratory boxplot analysis visually clarifies this stability, showing a tight alignment between the interquartile ranges (IQR) and median lines across all configurations. The absolute shifts across the entire topographic spectrum are systematically capped under a value of 0.9. Specifically, the lower drainage limits (P5) present an absolute difference of –0.4 (moving from –4.2 to –4.6), whereas the upper saturation limits (P95) display a variation of only –0.3 (from 2.7 to 2.4). Furthermore, the total standard deviation remains perfectly constant at 2.2 for both georeferencing scenarios, indicating that the structural roughness and overall statistical dispersion of the hydrological surfaces are not degraded by the omission of GCPs.

Table 4. Descriptive statistics of cell-by-cell Topographic Wetness Index (TWI) discrepancies between DJI Mavic 3M and DJI Matrice T4 photomorphometric models under different georeferencing configurations (With GCPs vs. Without GCPs), including absolute differences and relative changes (%)

Parameter	With GCPs	Without GCPs	Difference	Change (%)
Mean	-1.1	-1.5	-0.4	37.8
Median	-1.2	-1.7	-0.4	35.2
Minimum	-10.1	-11.0	-0.9	9.2
Maximum	19.8	20.7	0.9	4.6
Standard deviation	2.2	2.2	0.0	0.9
Coefficient of variation (%)	-207.2	-151.7	55.5	-26.8
Percentile 5 (P5)	-4.2	-4.6	-0.4	9.3
Percentile 25 (P25)	-2.4	-2.8	-0.4	17.7
Percentile 75 (P75)	0.0	-0.4	-0.4	1032.1
Percentile 95 (P95)	2.7	2.4	-0.3	-10.8

The local micro-topographic variations associated with surface convergence (drainage channels and gully systems) and divergence (crests and terrace boundaries) were evaluated utilizing the Convergence Index (CI) (Fig. 7 and Table 5). The spatial distribution of the CI limits highlights the highly complex geometric layout of the steep slope terraces. However, due to the presence of absolute minimum and maximum computational values constrained at the mathematical limits of –100.0 and 100.0, respectively, the cartographic visualization requires optimized local contrast stretching (between –20 and 20) to fully resolve the subtle linear features of the hillslope layout.

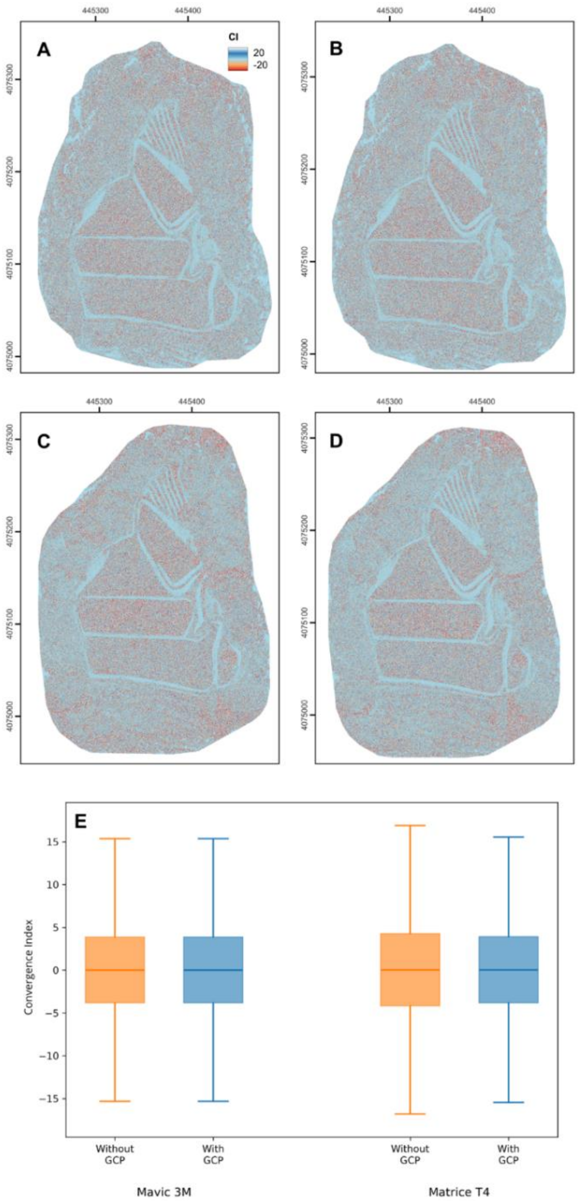

Figure 7. Comparison of Convergence Index (CI) maps and statistical distributions obtained from the four UAV photogrammetric workflows using RTK direct georeferencing and RTK combined with Ground Control Points (GCPs). (A) DJI Mavic 3 Multispectral (RTK only); (B) DJI Mavic 3 Multispectral (RTK + GCPs); (C) DJI Matrice T4 (RTK only); (D) DJI Matrice T4 (RTK + GCPs); (E) Boxplot comparison of Convergence Index (CI) distributions

The geostatistical residual matrix demonstrates an outstanding structural match between the digital elevation derivatives of both UAV systems. Under both georeferencing strategies ("With GCPs" and "Without GCPs"), the mean and median cell-by-cell CI discrepancies between the DJI Mavic 3M and DJI Matrice T4 remained locked at an absolute baseline of 0.0, yielding a net difference of 0.0. The extreme coefficients of variation recorded in the statistical summary (reaching –3,292,368.5% and –6,739,567.3%) do not indicate model instability; rather, they represent a well-known mathematical artifact triggered when dividing standard deviations by a global mean value that is practically zero, which is typical for balanced convergent/divergent landforms.

Table 5. Descriptive statistics of cell-by-cell Convergence Index (CI) discrepancies between DJI Mavic 3M and DJI Matrice T4 photogrammetric models under different georeferencing configurations (With GCPs vs. Without GCPs), including absolute differences and relative changes (%)

Parameter	With GCPs	Without GCPs	Difference	Change (%)
Mean	0.0	0.0	0.0	−47.9
Median	0.0	0.1	0.0	8.5
Minimum	−100.0	−100.0	0.0	0.0
Maximum	100.0	100.0	0.0	0.0
Standard deviation	11.9	12.7	0.8	6.6
Coefficient of variation (%)	−3292368.5	−6739567.3	−3447198.8	104.7
Percentile 5 (P5)	−17.0	−18.5	−1.5	9.1
Percentile 25 (P25)	−3.8	−4.2	−0.3	8.9
Percentile 75 (P75)	3.9	4.3	0.3	8.5
Percentile 95 (P95)	16.6	18.2	1.5	9.2

This absolute structural alignment is visually summarized in the exploratory boxplot analysis, where the interquartile ranges (IQR) and internal median indicators show perfect horizontal synchronization across all four scenarios. When evaluating the spatial distribution across the percentiles, the absolute discrepancies caused by omitting the ground control network remain exceptionally narrow. The intermediate terrain positions (P25 and P75) exhibit minor absolute deviations of only 0.3 (representing an 8.9% relative change baseline). Even at the extreme geometric boundaries of the terraced steps, represented by the 5th (P5) and 95th (P95) percentiles, the absolute inter-platform variations do not exceed 1.5 units.

Absolute Positioning Accuracy and Structural Block Behavior

To decipher the geometric nature of the errors, the absolute spatial coordinates (X, Y, Z) of 10 independent checkpoints were compared between the RTK direct georeferencing and the optimized GCP-supported workflows for both platforms (Table 6). The coordinate tracking reveals an identical, highly rigid systematic block shift across the study area rather than internal geometric distortion.

For the DJI Mavic 3M workflow, the direct RTK georeferencing introduced a uniform systemic offset, exhibiting a mean deviation of Delta X = 0.2 m, Delta Y = 5.3 m, and a vertical displacement of Delta Z = -2.8 m. The horizontal vector error remained locked at a constant 5.3 m. Tthe standard deviation for all directional components was 0.0 m, verifying that no internal warping or scale tilting occurred within the photogrammetric model. An identical pattern was captured with the DJI Matrice T4 platform. The structural model obtained a mean systematic translation of Delta X = 0.2 m, Delta Y = 5.4 m, and Delta Z = -2.8 m, resulting in a horizontal shift of 5.4 m. The internal coherence remained exceptionally high, with standard deviations capped between 0.0 m and 0.1 m across all checkpoints.

Table 6. Summary of absolute positioning errors and deviations (meters) at checkpoints

UAV Plaform	Metric	ΔX (m)	ΔY (m)	ΔZ (m)	Total Er-ror_X Y (m)
DJI Mavic 3M	Mean	0.2	5.3	-2.8	5.3
	Std. Dev.	0.0	0.0	0.0	0.0
DJI Matrice T4	Mean	0.2	5.4	-2.8	5.4
	Std. Dev.	0.0	0.1	0.1	0.1

This spatial behavior confirms a rigid-body translation artifact. The displacement is not an operational failure of the internal RTK modules; instead, it represents a standard datum or baseline reference initialization offset between the autonomous DJI D-RTK 3 broadcasting station and the post-processed multi-band Emlid Reach RS3 reference frame.

Discussion

The geomorphometric and pedogeomorphological implications of our results establish a new operational paradigm for monitoring high-energy agricultural landforms, such as the steep terraced vineyards evaluated in this study. The statistical distribution of the slope derivatives, RUSLE LS-factor, TWI, and Convergence Index (CI) demonstrated that next-generation RTK direct georeferencing achieves structural parity with traditional, labor-intensive Ground Control Point (GCP) networks. Across all four terrain indices, the median values and interquartile ranges remained almost unaltered between configurations, showing absolute discrepancies that rarely exceeded single-digit thresholds (e.g., a median slope variation of just 0.7° and an absolute mathematical variance of 0.0 in the structural boundaries of the Convergence Index). This high-performance internal consistency across the topographic spectrum proves that the micro-topography of terrace risers, flat benches, and developing gully systems can be modeled with identical morphological fidelity using either the compact DJI Mavic 3M or the heavy-duty DJI Matrice T4.

The physical explanation for this high geometric compliance is fully unraveled by the absolute checkpoint coordinate residual matrix. Instead of presenting localized photogrammetric warping, internal scale distortions, or vertical tilt—which are typical systematic errors associated with historical drone configurations—the pure RTK block acted as a perfectly rigid body (Rodrigo-Comino et al., 2026). The checkpoint analysis revealed an identical, systematic three-dimensional translation vector (ΔX≈0.2 m, ΔY≈5.4 m, and ΔZ≈-2.8 m) across the entire study site, accompanied by near-zero standard deviations (≤0.1 m) for both platforms. This spatial translation is an expected coordinate system calibration offset between the autonomous DJI D-RTK 3 base station and the post-processed Emlid Reach RS3 GNSS datum. Because the internal relative topography remains entirely unaffected by this rigid block shift, derivative calculations that rely on neighborhood cell algorithms—such as slope gradients, flow direction, and drainage accumulation—remain mathematically identical regardless of the absolute geographic anchoring.

This finding carries vital practical weight when contextualized within current vineyard degradation and UAV photogrammetry literature. Seminal studies in the Iberian Peninsula and Italy have heavily documented that steep terraced viticultural systems exhibit some of the most critical soil erosion rates, landslide vulnerabilities, and gully development processes due to structural abandonment or extreme rainfall events. Authors such as Romero-Díaz et al. (2017) in the Murcia region, Martínez-Casasnovas et al. (2016) in the Penedès region, and Rodrigo-Comino et al. (2019) in the Málaga province have consistently stressed the urgent need for high-resolution spatial tools to monitor these laderas before catastrophic soil loss occurs. Furthermore, on an international scale, researchers like Tarolli and Pijl have successfully utilized UAV photogrammetry in Italian terraced landscapes to detect and track active gully erosion and bank failures, confirming the extreme vulnerability of these agricultural systems (Pijl et al., 2022, 2020; Tarolli et al., 2015)).

However, executing traditional drone campaigns in these complex terrains is inherently inefficient and hazardous. As noted by classic authors in UAV methodologies (James et al., 2017; Turner et al., 2007), distributing and measuring dozens of physical targets (GCPs) across sub-vertical terrace walls introduces high operational risks, long fieldwork timelines, and significant economic costs. While recent evaluations of direct georeferencing workflows (Forlani et al., 2018; Benassi et al., 2017) have shown promising results for standard topographic tracking, their application in agricultural geometries of steep inclination remained unverified.

Our work successfully bridges this methodological gap by providing the first empirical evidence that direct RTK georeferencing via the DJI D-RTK 3 ecosystem completely eliminates the operational dependency on physical ground control for geomorphological monitoring. The lightweight Mavic 3M and the industrial Matrice T4 performed with equivalent geometric accuracy, proving that platform weight and sensor payloads do not degrade the internal consistency of the topographic models under identical flight constraints (40 m AGL, 80% overlap, solar noon). Consequently, this research establishes that managers and geomorphologists can confidently deploy direct RTK workflows to generate highly accurate risk maps, track active erosion channels, and design sustainable management practices in real time, bypassing the need for physical GCPs without losing any thematic or scientific rigor.

Furthermore, the clear interaction between the extracted geomorphometric parameters and the rigid body displacement results in key implications for predicting active surface hydrology in newly terraced mountain terrains. Because indices such as the TWI, CI, and RUSLE LS-factor rely entirely on relative neighborhood-cell pixel derivatives, the 5.4-meter horizontal and 2.8-meter vertical systematic translation vector does not distort the computed topographic flow paths. This explains why the resulting geomorphological maps remain virtually identical regardless of the GCP infrastructure. From an environmental perspective, this spatial consistency is highly valuable for anticipating the spatial activation of surface runoff and concentrated erosive processes, which are notoriously aggressive during the first high-intensity rainfall events on bare, newly prepared agricultural soils (Arnáez et al., 2017; Tarolli et al., 2015). By mapping these high-risk areas with direct RTK photogrammetry without the time-consuming constraints of ground control networks, land managers can rapidly identify critical connectivity pathways and design immediate mitigation strategies. In the context of our ongoing research, monitoring the site after upcoming rainfall events will establish an empirical baseline to assess nature-based solutions adapted to mountainous environments. Specifically, evaluating the strategic application of shredded pruning residues, grass cover or controlled, temporary animal grazing (e.g., targeted cover management via livestock) on the inner benches could provide a highly efficient mechanism to increase surface roughness, enhance infiltration, and curb initial runoff velocity, successfully mitigating soil and nutrient depletion before severe gully networks can develop (Mincu et al., 2025; Minea et al., 2019; Boardman & Vandaele, 2023; Centeri, 2022; Cerdà & Rodrigo-Comino, 2021).

Conclusions

This study allowed us to quantify the geometric and geomorphometric implications of utilizing direct RTK georeferencing workflows—bypassing traditional Ground Control Point (GCP) networks—for high-resolution mapping in newly steep terraced viticultural landscapes. By executing synchronized flight campaigns with the DJI Mavic 3M and DJI Matrice T4 platforms supported by the DJI D-RTK 3 base station, several critical conclusions can be drawn. The cell-by-cell algebraic comparison proved that advanced geomorphometric derivatives (Slope Gradient, TWI, Convergence Index, and RUSLE LS-factor) maintain structural parity regardless of GCP deployment. The core statistical distributions, interquartile ranges, and median thresholds remained virtually unaltered, validating that both platforms capture the intricate micro-topography of terrace risers and erosion channels with equivalent morphological fidelity. Checkpoint residual analysis unraveled that the unanchored RTK photogrammetric block behaves as a structurally rigid body. Rather than exhibiting local warping, horizontal scale distortions, or vertical tilting, the direct georeferencing workflow only introduced a uniform, systematic three-dimensional translation vector ($\Delta X \approx 0.2$ m, $\Delta Y \approx 5.4$ m, $\Delta Z \approx -2.8$ m) across the entire study site, maintaining near-zero standard deviations (≤0.1 m).

Because local geomorphological and hydrological indices are computed via spatial neighborhood matrices, their mathematical outputs are completely independent of absolute geographic anchoring. Consequently, the localized systematic block shift does not degrade the internal data quality or the interpretive capacity of the final geomorphological risk maps. The empirical evidence establishes that for localized pedogeomorphological tracking and agricultural risk modeling, the deployment of physical ground control targets can be confidently omitted. Bypassing GCP infrastructure significantly reduces field execution times, minimizes operational costs, and mitigates the physical risks associated with surveying sub-vertical terraced slopes. We concluded that this research provides a robust methodological endorsement for the implementation of direct RTK georeferencing in extreme agricultural geometries. It establishes a highly efficient framework for land managers and geomorphologists to monitor active soil degradation processes in real time, ensuring that scientific and thematic accuracy are fully preserved while operational workflows are thoroughly optimized.

Funding

This work was supported by Project: 101157354 — SOILCRATES; Horizon Europe (HORIZON; AMENDMENT No AMD-101157354-4). Also, parts of this research were funded by a 2021 Leonardo Grant for Researchers and Cultural Creators from the BBVA Foundation, for which we are deeply grateful. We also acknowledge the support from projects granted by the University of Granada within the Plan Propio: (i) PP2022.EI-01, "Caracterizando la degradación ambiental en el viñedo granadino. Un enfoque multidisciplinar a largo plazo utilizando parcelas experimentales y muestreos poblacionales"; 1 (ii) PPJIA2022-58, "Caracterización hídrica del suelo en viñedos para la optimización de recursos agrícolas y ambientales"; and (iii) Proyectos Innovadores 2022–2025 de Grupos Operativos AEI-agri (Andalucía): "Creación de una herramienta DSS (Decision Support System) para el manejo sostenible del suelo en viticultura." This research was also supported by the SOSVITI project—Sustainable Soil Management Decision Support System in Viticulture, funded under the Marie Skłodowska-Curie Staff Exchanges action within Horizon Europe 2030.

Author contribution

JG-V: Investigation, Visualization, Writing – original draft, Writing – review & editing. LC-R: Data curation, Visualization, Writing – original draft, Writing – review & editing. MTG-M: Data curation, Visualization, Writing – original draft, Writing – review & editing. JR-C: Conceptualization, Investigation, Resources, Data curation, Visualization, Supervision, Project administration, Funding acquisition, Writing – original draft, Writing – review & editing. All authors have read and agreed to the published version of the manuscript.

Conflicts of interest

The authors declare no conflict of interest.

References

Alexiou, S., Efthimiou, N., Karamesouti, M., Papanikolaou, I., Psomiadis, E., & Charizopoulos, N. (2023). Measuring Annual Sedimentation through High Accura-cy UAV-Photogrammetry Data and Comparison with RUSLE and PESERA Erosion Models. *Remote Sensing*, 15(5), 1339. https://doi.org/10.3390/rs15051339

Andrenelli, M.C., Pellegrini, S., Fila, G., Becagli, C., Valboa, G., & Vignozzi, N. (2025). Erosion Assessment by a Fast and Low-Cost Procedure in a Vineyard Under Different Soil Management. *Agriculture*, 15(21), 2218. https://doi.org/10.3390/agriculture15212218

Arabameri, A., Pradhan, B., Pourghasemi, H.R., Rezaei, K., & Kerle, N. (2018). Spatial Modelling of Gully Erosion Using GIS and R Programing: A Comparison among Three Data Mining Algorithms. *Applied Sciences*, 8(8), 1369. https://doi.org/10.3390/app8081369

Arnáez, J., Lana-Renault, N., Ruiz-Flaño, P., Pascual, N., & Lasanta, T. (2017). Mass soil movement on ter-raced landscapes of the Mediterranean mountain areas: A case study of the Iberian Range, Spain. *Cuadernos de Investigación Geográfica*, 43(1), 83-100. https://doi.org/10.18172/cig.3211

Barbera, G., & Cullotta, S. (2016). The Traditional Mediterranean Polycultural Landscape as Cultural Heritage: Its Origin and Historical Importance, Its Agro-Silvo-Pastoral Complexity and the Necessity for Its Identifica-tion and Inventory. In M. Agnoletti, & F. Emanueli (Eds.), *Biocultural Diversity in Europe* (pp. 21-48). Springer International Publishing. https://doi.org/10.1007/978-3-319-26315-1_2

Benassi, F., Dall'Asta, E., Diotri, F., Forlani, G., Morra di Cella, U., Roncella, R., & Santise, M. (2017). Testing Accuracy and Repeatability of UAV Blocks Oriented with GNSS-Supported Aerial Triangulation. *Remote Sensing*, 9(2), 172. https://doi.org/10.3390/rs9020172

Bertin, S., Stéphan, P., & Ammann, J. (2022). Assessment of RTK Quadcopter and Structure-from-Motion Photogrammetry for Fine-Scale Monitoring of Coastal Topographic Complexity. *Remote Sensing*, 14(7), 1679. https://doi.org/10.3390/rs14071679

Blavet, D., De Noni, G., Le Bissonnais, Y., Leonard, M., Maillo, L., Laurent, J.Y., Asseline, J., Leprun, J.C., Arshad, M.A., & Roose, E. (2009). Effect of land use and man-agement on the early stages of soil water erosion in French Mediterranean vineyards. *Soil and Tillage Re-search*, 106(1), 124-136. https://doi.org/10.1016/j.still.2009.04.010

Boardman, J., & Vandaele, K. (2023). Soil erosion and runoff: The need to rethink mitigation strategies for sustainable agricultural landscapes in western Europe. *Soil Use and Management*, 39(2), 673-685. https://doi.org/10.1111/sum.12898

Bogunovic, I., Telak, L.J., & Pereira, P. (2020). Exper-imental Comparison of Runoff Generation and Initial Soil Erosion Between Vineyards and Croplands of Eastern Croatia: A Case Study. *Air, Soil and Water Research*, 13, 1178622120928323. https://doi.org/10.1177/1178622120928323

Caffaro, F., Gregorio, E.D., Capello, G., Vigoroso, L., Bagagiolo, G., Cavallo, E., & Biddoccu, M. (2024). Wine-growers' Perceptions and Adoption of Sustainable Soil Management Practices and

Technologies: A Case Study in Piedmont, Italy. *Authorea*, 0716. https://doi.org/10.22541/au.172114304.44775604/v1

Cambronero, L., Yu, Y., & Rodrigo-Comino, J. (2025). Scaling up analysis of human impacts on hydrological connectivity in Mediterranean viticultural landscapes: From hillslope to a watershed perspective. *Ecohydrolo-gy & Hydrobiology*, 25(4), 100700. https://doi.org/10.1016/j.ecohyd.2025.100700

Centeri, C. (2022). Effects of Grazing on Water Erosion, Compaction and Infiltration on Grasslands. *Hydrology*, 9(2), 34. https://doi.org/10.3390/hydrology9020034

Cerdà, A., & Rodrigo-Comino, J. (2021). Regional Farmers' Perception and Societal Issues in Vineyards Affected by High Erosion Rates. *Land*, 10(2), 205. https://doi.org/10.3390/land10020205

Chen, D., Wei, W., & Chen, L. (2017). Effects of terracing practices on water erosion control in China: A meta-analysis. *Earth-Science Reviews*, 173, 109-121. https://doi.org/10.1016/j.earscirev.2017.08.007

Costa, J.M., Egipto, R., Aguiar, F.C., Marques, P., Nogales, A., & Madeira, M. (2023). The role of soil tem-perature in mediterranean vineyards in a climate change context. *Frontiers in Plant Science*, 14. https://doi.org/10.3389/fpls.2023.1145137

Desmet, P.J.J., & Govers, G. (1996). A GIS procedure for automatically calculating the USLE LS factor on topographically complex landscape units. *Journal of Soil and Water Conservation*, 51(5), 427-433. https://doi.org/10.1080/00224561.1996.12457102

Durán Zuazo, V., & Rodriguez, C. (2008). Soil-Erosion and Runoff Prevention by Plant Covers: A Review. *Agronomy for Sustainable Development*, 28. https://doi.org/10.1051/agro:2007062

Eltner, A., Mulsow, C., & Maas, H.-G. (2013). QUAN-TITATIVE MEASUREMENT OF SOIL EROSION FROM TLS AND UAV DATA. *The International Archives of the Pho-togrammetry, Remote Sensing and Spatial Information Sciences*, XL-1/W2, 119–124. https://doi.org/10.5194/isprsarchives-XL-1-W2-119-2013

Farella, M.M., Fisher, J.B., Jiao, W., Key, K.B., & Barnes, M. L. (2022). Thermal remote sensing for plant ecology from leaf to globe. *Journal of Ecology*, 110(9), 1996-2014. https://doi.org/10.1111/1365-2745.13957

Forlani, G., Dall'Asta, E., Diotri, F., Cella, U.M. di, Roncella, R., & Santise, M. (2018). Quality Assessment of DSMs Produced from UAV Flights Georeferenced with On-Board RTK Positioning. *Remote Sensing*, 10(2), 311. https://doi.org/10.3390/rs10020311

Gall, C., Oldenburg, S., Nebel, M., Scholten, T., & Seitz, S. (2025). Effects of moss restoration on surface runoff and initial soil erosion in a temperate vineyard. SOIL, 11(1), 199-212. https://doi.org/10.5194/soil-11-199-2025

García-Ruiz, J.M. (1988). La evolución de la agricultura de montaña y sus efectos sobre la dinámica del paisaje. https://digital.csic.es/handle/10261/100832

Gholamahmadi, B., Gonzalez Pelayo, O., Isaka, S., Campos, I., Martins, M., Bastos, A.C., Jongen, M., & Verheijen, F.G.A. (2025). The impact of biochar applica-tion on sponge function, water erosion, and vegetation cover in a Mediterranean vineyard soil. *Journal of Envi-ronmental Management*, 388, 125916. https://doi.org/10.1016/j.jenvman.2025.125916

González-Moreno, M.T., & Rodrigo-Comino, J. (2025). Geostatistical Vegetation Filtering for Rapid UAV-RGB Mapping of Sudden Geomorphological Events in the Mediterranean Areas. *Drones*, 9(6), 441. https://doi.org/10.3390/drones9060441

James, M.R., Robson, S., d'Oleire-Oltmanns, S., & Niethammer, U. (2017). Optimising UAV topographic surveys processed with structure-from-motion: Ground control quality, quantity and bundle adjustment. *Geomorphology*, 280, 51-66. https://doi.org/10.1016/j.geomorph.2016.11.021

Jenerowicz, A., Wierzbicki, D., & Kedzierski, M. (2023). Radiometric Correction with Topography Influence of Multispectral Imagery Obtained from Unmanned Aerial Vehicles. *Remote Sensing*, 15(8), 2059. https://doi.org/10.3390/rs15082059

Martínez-Casasnovas, J.A., Ramos, M.C., & Benites, G. (2016). Soil and Water Assessment Tool Soil Loss Simulation at the Sub-Basin Scale in the Alt Penedès–Anoia Vineyard Region (Ne Spain) in the 2000s. *Land Degrad. Develop.*, 27, 160–170. doi: 10.1002/ldr.2240

Mincu, F. I., Ortenzi, S., Di Matteo, L., Chendeş, V., Neculau, G., Ciobotaru, N., & Minea, G. (2025). The Validation of Soil Moisture Satellite Products Based on Hydrological Parameters Measured in a Small Basin, Romania. Journal of Water and Land Development, 52-60. https://doi.org/10.24425/jwld.2025.156039

Minea, G., Ioana-Toroimac, G., & Moroșanu, G. (2019). The dominant runoff processes on grassland versus bare soil hillslopes in a temperate environment—An experimental study. Journal of Hydrology and Hydromechanics, 67, 297-304. https://doi.org/10.2478/johh-2019-0018

Novara, A., Gristina, L., Saladino, S.S., Santoro, A., & Cerdà, A. (2011). Soil erosion assessment on tillage and alternative soil managements in a Sicilian vineyard. *Soil and Tillage Research*, 117, 140-147. https://doi.org/10.1016/j.still.2011.09.007

Pawlik, Ł. (2025). Geomorphic Data and Geomor-phometry Analyses. In Ł. Pawlik (Ed.), *R Applications in Earth Sciences: From Soil Data to Climate Time Series Analysis and Modeling* (pp. 81-91). Springer Nature Switzerland. https://doi.org/10.1007/978-3-031-89673-6_6

Pijl, A., Barneveld, P., Mauri, L., Borsato, E., Grigo-lato, S., & Tarolli, P. (2019). Impact of mechanisation on soil loss in terraced vineyard landscapes. *Cuadernos de*

Investigación Geográfica, 45(1), 287-308. https://doi.org/10.18172/cig.3774

Pijl, A., Reuter, L.E.H., Quarella, E., Vogel, T.A., & Tarolli, P. (2020). GIS-based soil erosion modelling under various steep-slope vineyard practices. *CATENA*, 193, 104604. https://doi.org/10.1016/j.catena.2020.104604

Pijl, A., Wang, W., Straffelini, E., & Tarolli, P. (2022). Soil and water conservation in terraced and non-terraced cultivations: An extensive comparison of 50 vineyards. *Land Degradation & Development*, 33(4), 596-610. https://doi.org/10.1002/ldr.4170

Preti, F., & Romano, N. (2014). Terraced landscapes: From an old best practice to a potential hazard for soil degradation due to land abandonment. *Anthropocene*, 6, 10-25. https://doi.org/10.1016/j.ancene.2014.03.002

Prosdocimi, M., Cerdà, A., & Tarolli, P. (2016). Soil water erosion on Mediterranean vineyards: A review. *CATENA*, 141, 1-21. https://doi.org/10.1016/j.catena.2016.02.010

Ramos, M.C., & Porta, J. (1997). Analysis of design criteria for vineyard terraces in the mediterranean area of North East Spain. *Soil Technology*, 10(2), 155-166. https://doi.org/10.1016/S0933-3630(96)00006-2

Rodrigo-Comino, J. (2018). Five decades of soil ero-sion research in "terroir". The State-of-the-Art. *Earth-Science Reviews*, 179, 436-447. https://doi.org/10.1016/j.earscirev.2018.02.014

Rodrigo-Comino, J., Seeger, M., Iserloh, T., Senciales González, J.M., Ruiz-Sinoga, J.D., & Ries, J.B. (2019). Rainfall-simulated quantification of initial soil erosion processes in sloping and poorly maintained terraced vineyards—Key issues for sustainable management systems. *Science of The Total Environment*, 660, 1047-1057. https://doi.org/10.1016/j.scitotenv.2018.12.451

Rodrigo-Comino, J., Xouris, C., Caballero-Calvo, A., Seeger, M., Kavian, A., & Kalogeras, A. (2026). From consumer to RTK-enabled UAVs: A comparative assess-ment of vineyard mapping accuracy and spectral indices. *Precision Agriculture*, 27(4), 90. https://doi.org/10.1007/s11119-026-10363-4

Romero-Díaz, A., Ruiz-Sinoga, J.D., Robledano-Aymerich, F., Brevik, E.C., & Cerdà, A. (2017). Ecosystem responses to land abandonment in Western Mediterra-nean Mountains. *CATENA*, Geoecology in Mediterranean mountain areas. Tribute to Professor José María García Ruiz, 149, 824-835. https://doi.org/10.1016/j.catena.2016.08.013

Tan, C., Chen, Z., Chen, Z., Liao, A., Zeng, X., & Cao, J. (2024). Accuracy analysis of UAV aerial photogramme-try based on RTK mode, flight altitude, and number of GCPs. *Measurement Science and Technology*, 35(10), 106310. https://doi.org/10.1088/1361-6501/ad5dd7

Tarolli, P., Sofia, G., Calligaro, S., Prosdocimi, M., Preti, F., & Dalla Fontana, G. (2015). Vineyards in Ter-raced Landscapes: New Opportunities from Lidar Data. *Land Degradation & Development*, 26(1), 92-102. https://doi.org/10.1002/ldr.2311

Trevisani, S., & Guth, P.L. (2025). Surface Roughness in Geomorphometry: From Basic Metrics Toward a Coherent Framework. *Remote Sensing*, 17(23), 3864. https://doi.org/10.3390/rs17233864